A 3D Interconnected Microchannel Network Formed in Gelatin by Sacrificial Shellac Microfibers

Published in final edited form as:
Adv Mater. 2012 October 2; 24(38): 5187–5191. doi:10.1002/adma.201200810.

A 3D interconnected microchannel network formed in gelatin by sacrificial shellac microfibers

Dr. Leon M. Bellan,
77 Massachusetts Avenue, The David H. Koch Institute, Room 76-661, Cambridge, MA 02139-4307

Matthew Pearsall,
77 Massachusetts Avenue, The David H. Koch Institute, Room 76-661, Cambridge, MA 02139-4307

Dr. Donald Cropek, and
U.S. Army Corps of Engineers, Construction Engineering Research Laboratory, Champaign, IL 61822

Prof. Robert Langer
77 Massachusetts Avenue, The David H. Koch Institute, Room 76-661, Cambridge, MA 02139-4307

Leon M. Bellan: Lbellan@mit.edu

Abstract

3D microfluidic networks are fabricated in a gelatin hydrogel using sacrificial melt-spun microfibers made from a material with pH-dependent solubility. The fibers, after being embedded within the gel, can be removed by changing the gel pH to induce dissolution. This process is performed in an entirely aqueous environment, avoiding extreme temperatures, low pressures, and toxic organic solvents.

Keywords

vascular; hydrogel; gelatin; shellac; microfiber

Traditional microfluidic device fabrication techniques predominantly produce patterns with two dimensional complexity suitable for manufacturing devices that rely on exact placement of functional elements. However, there are many applications within the realm of materials that have less stringent demands on pattern accuracy but require a microfluidic architecture with three dimensional extent and complexity. Natural systems, such as animal and plant vascular systems, are excellent examples of the potential of 3D microfluidic networks for materials applications. Engineered materials containing microfluidic networks have shown promise as self-healing materials,[1][2] internally cooled materials,[3] and constructs for regenerative medicine and bioengineering purposes.[4] [6] Due to their high surface area, 3D microfluidic networks could also prove useful for drug delivery, artificial lungs[7] [9] and energy harvesting applications based on microfluidic designs.[10] [12] However, in addition to the difficulty encountered when scaling microfluidic fabrication to 3D, bioinspired and biomimetic material fabrication is limited by the lack of a robust set of processes for

Correspondence to: Leon M. Bellan, Lbellan@mit.edu.

Supporting Information is available online from Wiley InterScience or from the author.

fabricating channels in biomimetic materials with high water content (hydrogels). Such materials are expected to have diffusive properties similar to naturally occurring materials of high water content. Using sacrificial shellac microfibers produced with a commercial cotton candy machine, we have formed a 3D microchannel network in a gelatin hydrogel. By exploiting the pH-sensitive solubility of shellac, we are able to remove the microfiber network by an entirely aqueous fabrication process, avoiding extreme temperatures and pressures, as well as toxic organic solvents. The large-scale microfluidic hydrogels created with this technique enable a wide range of applications requiring a macroscopic material in which transport of soluble entities occurs both via diffusion (through an aqueous gel) and advection (via flow through a 3D microchannel network).

Previous efforts devoted to the fabrication and characterization of artificial vascular networks often exploited microfluidic device fabrication techniques (photolithography, thin film deposition and etching, etc.) borrowed from the semiconductor industry. These techniques have been used to form planar vascular networks,[13] [15] which may then be stacked to produce 3D patterned channel networks.[16] [18] However, to achieve the 3D channel densities necessary to replicate natural vascular networks, a large number of very thin patterned layers would need to be aligned and stacked. The impracticality of this process has prevented the use of multilayer stacking to produce 3D microfluidic systems with high 3D channel density. Recently, non-traditional approaches to fabricating complex 3D fluidic systems have been presented (sacrificial microfiber networks[19] and electric discharge[20]), each sacrificing the accuracy of traditional lithographic techniques for scalability. Such high channel density architectures are able to deliver soluble compounds to a large volume.[21] Another recent non-traditional technique exploited sacrificial materials woven through a fibrous matrix to form patterned microfluidic structures with periodic Z position.[3] To date, however, these techniques have only been used to fabricate channels in solid materials.

While several techniques have been applied to form microfluidic structures in solid materials, the number of processes available for fabrication of microfluidic channels in hydrogels is limited. Hydrogel materials are much more difficult to process, as they are often mechanically fragile, unable to be exposed to extreme temperatures or low pressures, and may be incompatible with harsh chemical treatments. Early work in this area demonstrated techniques for producing 2D microfluidic networks in alginate[4] and agarose.[5] Simple single, non-branching, fluidic channels have been formed in hydrogels by pouring the hydrogel precursor over a thin needle, which is subsequently withdrawn after the gel has set.[22] More recently, direct write techniques employing material dispensed from a syringe on a 3-axis stage have been used to form a fluidic system in a Pluronic hydrogel.[23] Collagen constructs patterned with microchannels have also been investigated as implantable materials that can direct cellular invasion.[24] However, researchers have yet to demonstrate a complex high density 3D channel network throughout a thick slab of hydrogel, a milestone necessary for the production of thick prevascularized soft tissue constructs or other large scale biomimetic microfluidic materials.

To overcome both the hurdles of 3D channel network fabrication and fabrication within hydrogels, we have employed a strategy exploiting sacrificial melt-spun microfiber networks formed from a material with pH-dependent solubility. This strategy allowed us to “trigger” the dissolution by simply changing the pH under relatively mild conditions. We were thus able to maintain an aqueous fabrication process, avoiding organic solvents, extreme temperatures, or non-atmospheric pressures. Because the sacrificial structures were of varying sizes (ranging from interfacing macrostructures of several millimeter diameter to microfibers with diameters in the 10μm range) and thus of varying surface-to-volume ratios, simply using a slowly dissolving material seemed impractical. Briefly, a sacrificial structure

was built from melt-spun shellac microfiber networks and larger shellac structures deposited with a hot glue gun (Figure 1A). The sacrificial structure was embedded within enzymatically-crosslinked gelatin. When the gelatin had gelled, the sacrificial structure was removed by immersing the composite structure in a warm ammonia bath, leaving an intricate network of microchannels connected to a macrochannel (Supplemental Video 1). The shellac microfibers are highly autofluorescent (Supplemental Video 2), and the almost complete absence of this autofluorescence after the completion of the fabrication process (Supplemental Video 3) indicates that the sacrificial material has almost entirely dissolved. It is likely, however, that residual shellac remains in the material both as undissolved particulates (shellac is a thermoset and can crosslink to form insoluble material) and as dissolved shellac trapped within the gel volume (this can be seen by eye as subtle coloration throughout the finished construct, this coloration is not seen in pure hydrogel processed identically but without any embedded sacrificial material).

To interface to the macrochannels, we glued NanoPorts (Upchurch Scientific) directly to the hydrogel using a cyanoacrylate glue (Loctite 4541) (Figure 1B). This process allowed us to form a robust seal between the inlet macrochannel and external tubing; this connection was limited in strength by the fragility of the hydrogel. At times when the seal did leak, we noted that it was because of a rip in the hydrogel, and not a failure at the hydrogel-glue or glue-nanoport interface. FluoSpheres were introduced into the channel network to allow imaging of the channel architecture (Supplemental Video 4). Optical sectioning fluorescence microscopy was used to obtain 3D datasets of FluoSphere-filled channels. This data was used both for 3D channel visualization (Figure 2 and Supplemental Video 5) as well as to quantitatively characterize the channel system architecture.

The fluidic resistance of the microfluidic systems within the gelatin hydrogel was characterized as described previously,[21] and the resulting values for the six constructs tested ranged from 0.2 to 1.1 psi min mL^{-1}. These values are similar to the vascular resistance of some human tissue flaps used for reconstructive surgery.[25][26]

The microfiber diameters, determined by the melt-spinning temperature and rotational rate, define the resulting channel diameters. Similarly, the packing density of the microfibers when placed in the silicone mold (a manual process in this study) determines the interchannel distance. Because the melt-spun microfibers are not of a well-defined size or density, it is important to quantitatively characterize the channel architecture they produce. We sought to characterize two aspects of the channel network: channel size and interchannel distance. To characterize the channel size in a quantitative fashion, we first skeletonized the 3D channel dataset (Supplemental Video 6), and then used the resulting channel centerlines to mask a dataset consisting of the distance from each point within a channel to the channel wall. The result of this analysis is a dataset consisting of points only on channel centerlines, with values that indicate the largest sphere, centered at a point on a channel centerline, which can fit within the channel. Thus each point on the channel centerlines is assigned a radius. To characterize the interchannel distance, each point exterior to the channels was assigned a value indicating the shortest 3D distance between the point and a channel wall. Histograms containing data from 5×10^9 total cubic voxels, each with edge length of 1.24μm, are shown in Figure 3. Each dataset consisted of a stack several hundred images of 1024px × 1024px (several hundred μm thick × 1.27mm × 1.27mm)

The distributions shown in Figure 3 can be compared to data from similar analyses of natural vascular systems. Recently, Cassot et al published a study detailing the measurement and analysis of microvascular networks in the human cerebral cortex.[27] This in-depth analysis included skeletonizing the 3D dataset and determining channel diameters using methods similar to those used in the current study. The study by Cassot et al determined a

wide range of quantitative measurements of the network architecture, including a frequency distribution of diameters (Figure 5 in Cassot et al) showing a mean diameter value of approximately 7μm (two datasets, 6.91±3.85μm and 7.72±3.30μm). Our channel diameter dataset presented in Figure 3A has a mean diameter of 17μm and standard deviation of 19μm. Moreover, over 70% of the measured interchannel voxels are within 80 voxels (100μm; the approximate diffusion-limited maximum distance between a cell and a capillary[28]) of a channel (Figure 3B). Because the fiber networks are manually packed into the silicone molds used to form devices, the channel density is not well controlled in our current study; more automated versions of this fabrication process could remedy this.

The ability of the channel diameter analysis to correctly provide the distribution of channel diameters within devices depends on proper skeletonization of the channel network. Observation of the skeleton dataset overlaid on the original network dataset reveals that the skeletonization is quite good, and in most places correctly identifies centerlines of channels. Each dataset was checked for this correlation. There are two common ways in which the skeletonization processing incorrectly identifies centerlines. First, small branches, tangent to the centerline (i.e. in a radial direction) sometimes remain on the skeleton; this is extremely rare and only occurs on larger channels. Second, very large channels can appear to be non-uniformly fluorescing due to an increased number of FluoSpheres adhering to the channel walls. This causes a filled channel to appear as a hollow tube in the thresholded dataset, and thus yields an incorrect centerline. This error, as well, is rare. The rarity of these errors suggests the diameter distribution yielded by the analysis is representative of the actual distribution, though it is likely that larger channels may be under-represented due to the second type of error. There is also an inherent error in the pore size characterization due to the finite size of each dataset. It should be noted that Cassot et al validated their skeletonization quantitatively (using knowledge about a natural vascular network that cannot be assumed for our fabricated network, such as assuming channels shouldn't end and shouldn't be multiple-connected) and determined that their processing yielded a skeleton that was almost 90% correct.

In summary, we have presented a process to form 3D microfluidic networks in hydrogels by exploiting a sacrificial melt-spun material with pH-dependent solubility. The microfluidic networks had large extent (on the order of 1cm in all three dimensions), and could be made larger if desired. The macroscopic shape of the final hydrogel structure was defined by the silicone mold used, and shapes more complex than the rectangular prisms produced in this work could be formed using more complex silicone molds. The process described herein produces an inherently 3D architecture that cannot practically be formed using conventional microfabrication techniques, in a material system that is traditionally difficult to pattern. We also demonstrated a robust yet simple method to form a strong interface between hydrogels and external tubing. Using 3D datasets of the channel architecture, we characterized the channel diameter and interchannel distance distribution. This characterization yielded results that compare well with quantitative analyses of natural microvascular systems. Non-traditional 3D microfabrication strategies such as the process described herein will enable the production of novel microfluidic materials for bioengineering, structural, and energy applications.

Experimental

Construct Fabrication

Constructs were formed using a technique utilizing sacrificial microfiber networks described previously.[19] The previous work described the fabrication of such networks in PDMS, epoxy, and polycaprolactone, but the sugar-based fibers used would not be able to withstand being embedded in a hydrogel precursor solution due to the high water content. Thus, the

sacrificial material was switched to shellac, a natural material that exhibits pH-sensitive solubility in aqueous solutions and has appropriate mechanical properties, melt temperature and viscosity. The microfiber networks in the current study were collected manually from a cotton candy machine (The Helman Group, CCM-505) modified with two variacs to allow control of temperature and extractor head speed. To best produce microfibers from shellac, the temperature variac was set to ~70% and the extractor head speed variac was set to ~60%. Shellac (SSB 55, SSB Stroever Schellack Bremen) was milled (IKA works, model A11) and an appropriate quantity was placed in the heated extractor head. Shellac produced a 3D fibrous material similar in appearance to sugar-based cotton candy. We noticed that shellac is able to produce fibers over a wider range of parameters than sugar, allowing one to tune the fiber diameter range substantially (Supplemental Figure 1) or obtain a fiber network with a wide distribution of fiber diameters.[29] The shellac microfiber network (~0.5–0.75g) was manually placed in a silicone mold of 3cm x 3cm and confined to a height of ~2cm. To form the inlet and outlet channels, thicker sticks of shellac (~0.25g each) were extruded directly onto the fiber network using glue gun and a metal rod to push through shellac powder. The mold was then placed in a sealed plastic box with a small amount of ethanol. The box was placed in an incubator at 37C for 15 minutes to expose the shellac structure to ethanol vapor, making the structure temporarily tacky and improving interconnectivity between strands.

The hydrogel chosen for the scaffold material was enzymatically-crosslinked gelatin. To form the hydrogel, gelatin (type A from porcine, Sigma) was dissolved in sterile PBS (without Ca or Mg) at a concentration of 5%. The solution was placed in a water bath at 37C until the gelatin fully dissolved. A sterile solution of 10% microbial transglutaminase (mTG) (Activa-TI, Ajinomoto) in water was prepared using a 0.2μm filter. The enzyme solution was added to the gelatin solution at a ratio of 1:10, and the liquid was shaken vigorously to mix the two. To remove air bubbles, the solution was briefly sonicated in a water bath sonicator. Finally, the gelatin solution containing enzyme was poured slowly over the shellac structures in the silicone mold until the structures were fully immersed. The molds were placed in a humid incubator at 37C to allow the gelatin to crosslink overnight. The gelatin/shellac composite was then removed from the molds, and thin slices of material were removed from several of the exposed surfaces to expose shellac cross-sections. To sacrifice the shellac structure, the gelatin/shellac composite was placed in a stirred bath of ~850mL water containing 2.5mL ammonium hydroxide at 60C overnight (one ~20mL gelatin device containing roughly 1–1.25g shellac per bath, leading to an estimated 1cm^3 total channel volume assuming negligible swelling and a shellac density[30] of 1.1g/cm^3). The next day, the water/ammonium bath was replaced with fresh solution, and after 2 hours the bath was again replaced with pure DI water. After 30 minutes, the devices were transferred to beakers containing 1.8L DI water (one ~20mL gelatin device per beaker) and autoclaved for 20 minutes on a liquid cycle. The now-sterile devices were then removed from the autoclaved water in a sterile cell culture hood and transferred to 400mL sterile PBS storage bath (one device per bath). Devices were then stored at room temperature until used.

Fluidic Resistance Characterization

The fluidic resistance of several devices was characterized by flowing water into an inlet macrochannel at a known flow rate (New Era NE-300 syringe pump with a 3mL syringe) and measuring the pressure buildup at the inlet (Omega DP25B-S strain meter with a Honeywell 26PCAFG6G 1PSI flow-through pressure sensor). The fluidic resistance of the tubing was first measured (~0.1 psi min mL^{-1}) at flow rates ranging up to 800μL/min. Then the fluidic resistances of several devices were measured at flow rates ranging up to 120μL/min. For each device, several flow rates were used in random order, and between each measurement at a given flow rate, the flow was stopped and the pressure allowed to return to zero. For each device dataset, a line was fit to the pressure vs flow rate data, and the fluidic

resistance was reported as the slope of the line minus the tubing resistance. No leaking was observed at the inlet channel seal.

Imaging and Data Processing

Devices were imaged using a variety of techniques. Fluorescence video microscopy (Zeiss Axiovert 200m microscope, 5x Fluar objective) was used to demonstrate flow in the channel system. To obtain accurate 3D imaging data, an Olympus FV1000 multiphoton microscopy system, employing a MaiTai DeepSee HP laser and a 10x XLUMPlanFl objective, was used to image devices filled with an aqueous solution of 20nm red FluoSpheres diluted 1:100 from the stock solution. The resulting image stacks were reconstructed in 3D using BioView 3D (for pure visualization)[31] and the FIJI ImageJ package (for analysis)[32][33]. To quantify the channel diameters and inter-channel spacing, the multiphoton images were processed using a series of ImageJ plugins. First, the dataset was smoothed in 3D using a Gaussian filter with a sigma value of 2. The data was then thresholded (using the Li algorithm of the Auto Threshold plugin). Small specks (radius threshold of 3) and holes (radius threshold of 5) were eliminated using the Remove Outliers plugin. The resulting binary data was skeletonized in 3D using the Skeletonize3D plugin.[34] The AnalyzeSkeleton plugin[34] was then used to break loops and prune short branches. To construct the distance map dataset, the original dataset was first thresholded (using the Li algorithm of the Auto Threshold plugin), and removed of outliers as before. The Geometry to Distance Map plugin[35] was then used to construct a dataset in which the value of each point describes the distance from that point to an edge. To obtain quantitative information about the channel diameters, the centerlines obtained from the skeletonization were used to mask the results of the distance calculation, resulting in a dataset where the only non-zero voxels were channel centerlines, and where each non-zero voxel value corresponded to the largest sphere that could fit at that point. All zero-valued pixels were set to NaN (“not a number”) so they would not show up in the analysis. A histogram was then calculated. Similarly, to quantify the interchannel spacing, the Geometry to Distance Map plugin was used on the inverse of the thresholded dataset, and a histogram of the resulting 3D dataset was obtained (again without zero-valued pixels).

Supplementary Material

Refer to Web version on PubMed Central for supplementary material.

Acknowledgments

The authors wish to thank Ignacio Arganda-Carreras for help with the AnalyzeSkeleton plugin, and Dr. Jeffrey Borenstein for the use of the pressure measurement apparatus. This research was supported in part by the U.S. Army Engineer Research and Development Center Construction Engineering Research Laboratory (ERDC-CERL), and in part by Cancer Center Support (core) Grant P30-CA14051 from the NCI. One of the authors, LMB, gratefully acknowledges support from NIH grants F32EB011866 and K99EB013630.

References

1. Toohey KS, Sottos NR, Lewis JA, Moore JS, White SR. Nat Mater. 2007; 6:581–585. [PubMed: 17558429]
2. Hansen CJ, Wu W, Toohey KS, Sottos NR, White SR, Lewis JA. Adv Mater. 2009; 21:4143–4147.
3. Esser-Kahn AP, Thakre PR, Dong H, Patrick JF, Vlasko-Vlasov VK, Sottos NR, Moore JS, White SR. Advanced Materials. 2011; 23:3654–3658. [PubMed: 21766345]
4. Cabodi M, Choi NW, Gleghorn JP, Lee CSD, Bonassar LJ, Stroock AD. J Am Chem Soc. 2005; 127:13788–13789. [PubMed: 16201789]
5. Ling Y, Rubin J, Deng Y, Huang C, Demirci U, Karp JM, Khademhosseini A. Lab Chip. 2007; 7:756. [PubMed: 17538718]

6. Golden AP, Tien J. Lab Chip. 2007; 7:720. [PubMed: 17538713]
7. Burgess KA, Hu HH, Wagner WR, Federspiel WJ. Biomed Microdevices. 2008; 11:117–127. [PubMed: 18696229]
8. Potkay JA, Magnetta M, Vinson A, Cmolik B. Lab on a Chip. 2011; 11:2901. [PubMed: 21755093]
9. Kniazeva T, Hsiao JC, Charest JL, Borenstein JT. Biomed Microdevices. 2011; 13:315–323. [PubMed: 21113664]
10. Lei L, Wang N, Zhang XM, Tai Q, Tsai DP, Chan HLW. Biomicrofluidics. 2010; 4:043004.
11. Borno RT, Steinmeyer JD, Maharbiz MM. Applied Physics Letters. 2009; 95:013705.
12. Krupenkin T, Taylor JA. Nature Communications. 2011; 2:448.
13. Fidkowski C, Kaazempur-Mofrad MR, Borenstein J, Vacanti JP, Langer R, Wang Y. Tissue Engineering. 2005; 11:302–309. [PubMed: 15738683]
14. Shin M, Matsuda K, Ishii O, Terai H, Kaazempur-Mofrad M, Borenstein J, Detmar M, Vacanti JP. Biomedical Microdevices. 2004; 6:269–278. [PubMed: 15548874]
15. Borenstein JT, Tupper MM, Mack PJ, Weinberg EJ, Khalil AS, Hsiao J, García-Cardeña G. Biomed Microdevices. 2009; 12:71–79. [PubMed: 19787455]
16. Borenstein JT, Weinberg EJ, Orrick BK, Sundback C, Kaazempur-Mofrad MR, Vacanti JP. Tissue Engineering. 2007; 13:1837–1844. [PubMed: 17590149]
17. King KR, Wang CCJ, Kaazempur-Mofrad MR, Vacanti JP, Borenstein JT. Advanced Materials. 2004; 16:2007–2012.
18. Marentis TC, Vacanti JP, Hsiao JC, Borenstein JT. J Microelectromech Syst. 2009; 18:531–538.
19. Bellan LM, Singh SP, Henderson PW, Porri TJ, Craighead HG, Spector JA. Soft Matter. 2009; 5:1354–1357.
20. Huang JH, Kim J, Agrawal N, Sudarsan AP, Maxim JE, Jayaraman A, Ugaz VM. Adv Mater. 2009; 21:3567–3571.
21. Bellan LM, Kniazeva T, Kim ES, Epshteyn AA, Cropek DM, Langer R, Borenstein JT. Advanced Healthcare Materials. 2012; 1:164–167. [PubMed: 22708076]
22. Nichol JW, Koshy ST, Bae H, Hwang CM, Yamanlar S, Khademhosseini A. Biomaterials. 2010; 31:5536–5544. [PubMed: 20417964]
23. Wu W, DeConinck A, Lewis JA. Adv Mater. 2011; 23:H178–H183. [PubMed: 21438034]
24. Zheng Y, Henderson PW, Choi NW, Bonassar LJ, Spector JA, Stroock AD. Biomaterials. 2011; 32:5391–5401. [PubMed: 21549426]
25. Mahabir R, Williamson J, Carr N, Courtemanche D. Annals of Plastic Surgery. 2001; 47:148. [PubMed: 11506322]
26. Takanari K, Kamei Y, Toriyama K, Yagi S, Torii S. J Reconstr Microsurg. 2009; 25:39–45. [PubMed: 18942044]
27. Cassot F, Lauwers F, Fouard C, Prohaska S, Lauwers-Cances V. Microcirculation. 2006; 13:1–18. [PubMed: 16393942]
28. Kannan RY, Salacinski HJ, Sales K, Butler P, Seifalian AM. Biomaterials. 2005; 26:1857–1875. [PubMed: 15576160]
29. Bursac N, Loo Y, Leong K, Tung L. Biochem Biophys Res Commun. 2007; 361:847–853. [PubMed: 17689494]
30. Rowe, RC.; Sheskey, PJ.; Quinn, ME., editors. Amer Pharmaceutical Assn. 2009. Handbook of Pharmaceutical Excipients.
31. Kvilekval K, Fedorov D, Obara B, Singh A, Manjunath B. Bioinformatics. 2010; 26:544. [PubMed: 20031971]
32. Rasband, WS. ImageJ. U. S. National Institutes of Health; Bethesda, Maryland, USA: 1997–2012. Http://imagej.nih.gov/ij/n.d
33. Schindelin, J. Fiji Is Just ImageJ (batteries Included). ImageJ User and Developer Conference; Luxembourg. 2008.
34. Arganda-Carreras I, Fernández-González R, Muñoz-Barrutia A, Ortiz-De-Solorzano C. Microscopy Research and Technique. 2010; 73:1019–1029. [PubMed: 20232465]
35. Dougherty R, Kunzelmann KH. Microscopy and Microanalysis. 2007; 13:1678–1679.

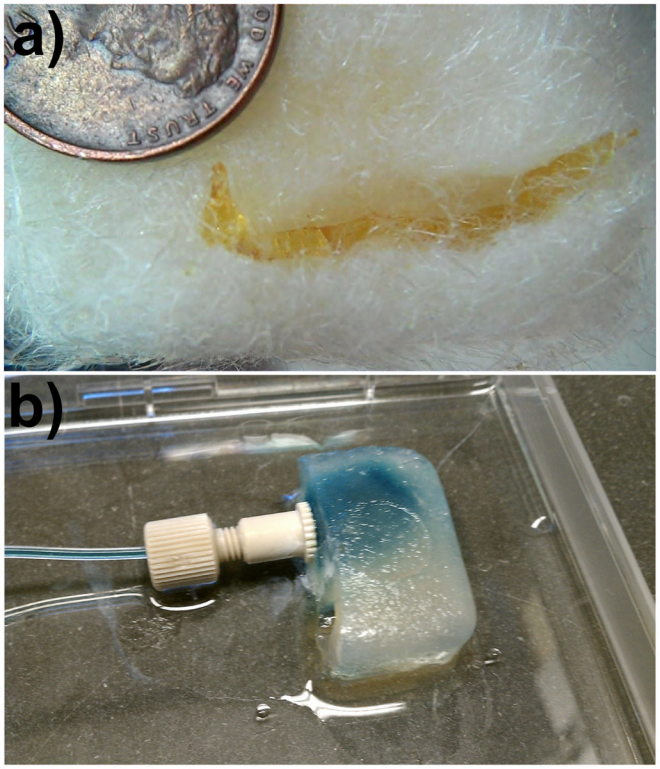

Figure 1.
A) Melt spun shellac microfiber network with a larger piece of shellac (dark yellow) extruded on top. A U.S. penny is shown for size reference. B) Gelatin construct connected to external tubing using a NanoPort attached with cyanoacrylate glue. Blue food coloring was introduced into the macrochannel and has started to propagate through the microchannels and diffuse through the hydrogel.

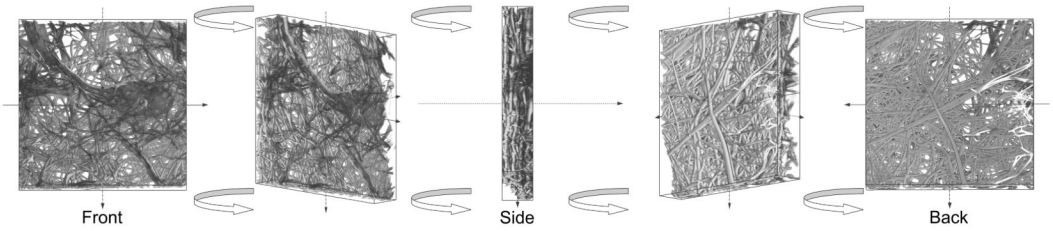

Figure 2.

A sequence of images from 3D reconstruction of multiphoton microscopy of FluoSphere-filled microchannels (Supplemental Video 5). Each rotation is 45 degrees. This dataset is 1.27mm wide x 1.27mm tall x 236μm deep.

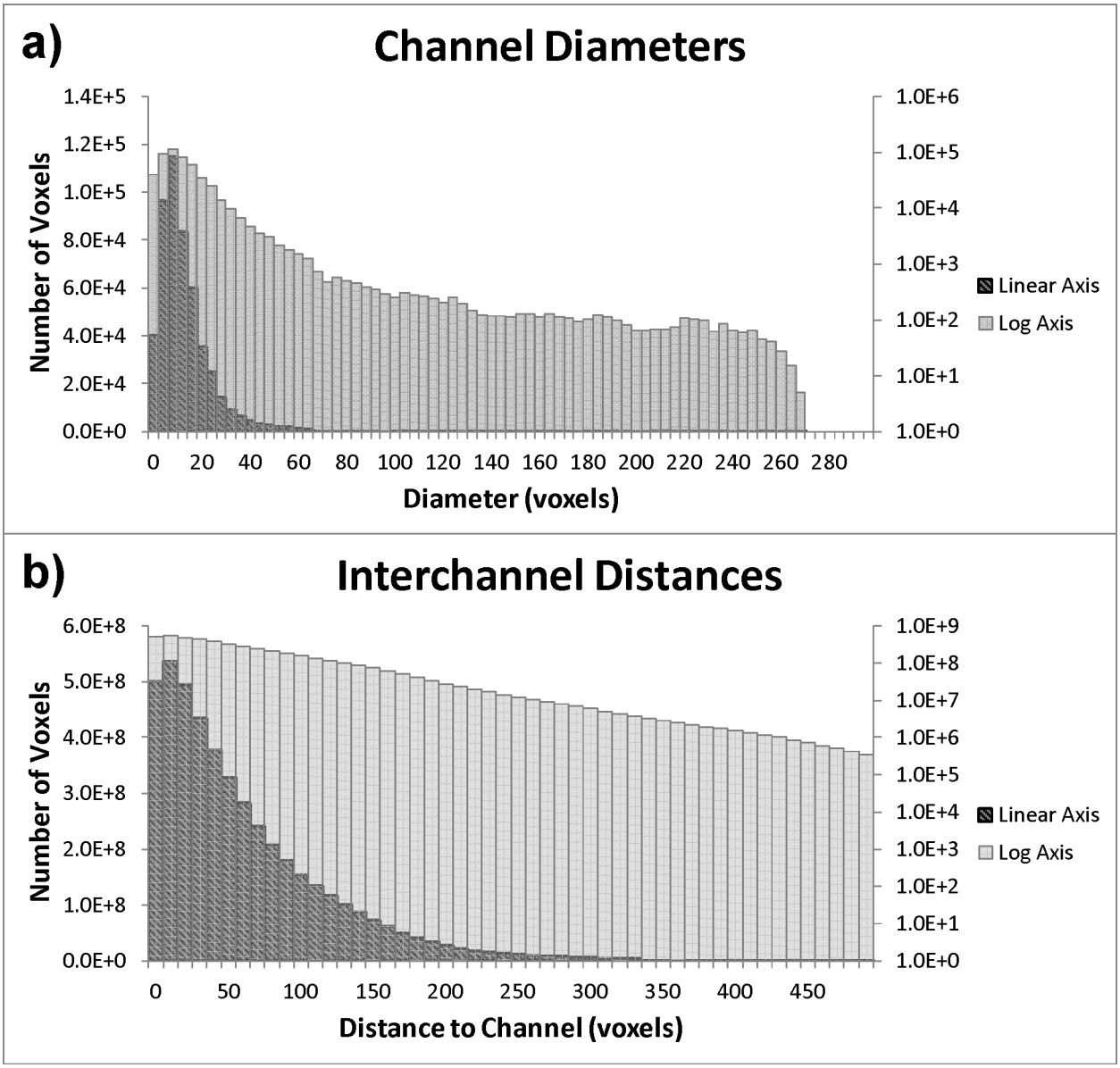

Figure 3.
Distribution of A) channel diameters (4.7×10^5 centerline voxels total) and B) interchannel distances (4.7×10^9 interchannel voxels total).